MgB_2線実用化のための基礎開発

低温センター基礎開発報告会

2007.06.01

鈴木敏一

2005~2006

- 原料微粒子化で充填率向上の検討
  - サブミクロン粒子化->Jc向上の例
  - ナノ粒子の焼結温度低下
    - B Tmp=2579℃, Tbp=3931℃
  - 表面酸化物層の影響が大きい
- 低酸素分圧での原料粉品質の向上検討
  - 原理的には高温で還元可能
  - 極低酸素分圧雰囲気を作れば低温でも還元可能
  - ジルコニアセラミックスを使った酸素ポンプ応用
    - p_{O2} ~ 10^{-24} atom @ 800℃の真空炉

MgB_2の超伝導性発見

AlB_2型構造を持つ金属間化合物として既知の物質であったが2001年に
青山学院大グループが転位温度39Kの超伝導物質であることを発見した
（Nature 410 (2001) 63）

letters to nature

By making the rotating wave approximation[19], we find equations with analytic solutions for the resonant case. The conductivity induced by a rectangular pulse of duration τ is taken to be proportional to $(1-\rho_{11}(\tau))$, the total number of donors excited out of the ground state at the end of the terahertz pulse. The solid curves in Fig. 3a are a least-squares fit of the data to this analytic solution. The fitted curves reproduce the essential features of the data.

The inset to Fig. 3a shows the Rabi frequency and damping rates extracted from the fits as functions of E_{THz}. If we assume a dipole matrix element of 10 nm, then the Rabi frequency at a terahertz field of 3.1×10^4 V m^{-1} is predicted to be 4.7×10^{11} rad s^{-1}, well within experimental error of the observed value. The fitted Rabi frequency increases roughly linearly with E_{THz} but with a non-zero intercept. The magnetic field was tuned to be resonant at the highest E_{THz}. The non-zero intercept is consistent with the detuning that results from the shift in the resonance frequency with E_{THz} (see Fig. 3b).

We calculated the curves in Fig. 4b by fixing the model parameters with a fit to the on-resonance curve, and varying only the detuning for the off-resonance curves. The frequency of the oscillations in the theoretical curves increases with increasing detuning, while the amplitude decreases, as observed in the experiment; however, we note that the amplitude decreases much more quickly with detuning in the experiment.

The mechanisms that damp the observed Rabi oscillations are extrinsic to the model qubits, and much faster than predicted intrinsic decoherence. The value of the dephasing rate γ_2 at the lowest terahertz field is, within experimental error, the same as that obtained from the linear spectra, 60×10^9 s^{-1}. This regime is inhomogeneously broadened by a background disorder potential[16]. As the terahertz field is increased, the inset to Fig. 3a shows γ_2 and γ_3 increasing, consistent with a photoionization process that couples the $2p^+$ state to a higher excited state. Intrinsic decoherence of motional states of hydrogenic impurities is expected to be limited by very weak coupling to acoustic phonons[20–24]. From table III of ref. 23, the contribution of acoustic-phonon coupling to the line-width (full-width at half-maximum, FWHM) of the $1s-2p$ ($m = 0$) transition at zero magnetic field is predicted to be $\leqslant 10^{-3}\Xi^2/(\rho a^3 v^2) \approx 0.2\,\mu$eV (where $\Xi = 8.6$ eV is the deformation potential, $a = 10$ nm is the Bohr radius, $\rho = 5{,}300$ kg m^{-3} is the density, and $v = 3{,}700$ m s^{-1} is the velocity of sound, corresponding to an intrinsic decoherence rate $\gamma_2 \leqslant 2 \times 10^8$ s^{-1}. Such decoherence rates, more than 1,000 times slower than typical Rabi frequencies measured here, would enable more complex manipulations of the model qubits. Future experiments will attempt to measure the intrinsic decoherence time of $2p$ ($m = -1$) hydrogenic donor states, which are well below the continuum and hence robust to ionization by photons and phonons. □

Received 5 December; accepted 18 December 2000.

1. Loss, D. & DiVincenzo, D. P. Quantum computation with quantum dots. *Phys. Rev. A* **57**, 120–126 (1998).
2. Kane, B. E. A silicon-based nuclear spin quantum computer. *Nature* **393**, 133–137 (1998).
3. Sherwin, M. S., Imamoglu, A. & Montroy, T. Quantum computation with quantum dots and terahertz cavity quantum electrodynamics. *Phys. Rev. A* **60**, 3508–3514 (1999).
4. Imamoglu, A. *et al.* Quantum information processing using quantum dot spins and cavity QED. *Phys. Rev. Lett.* **83**, 4204–4207 (1999).
5. Vrijen, R. *et al.* Electron spin resonance transistors for quantum computing in silicon-germanium hetero-structures. Preprint quant-ph/9905096 at (http://xxx.lanl.gov) (1999).
6. Bennett, C. H. & DiVincenzo, D. P. Quantum information and computation. *Nature* **404**, 247–255 (2000).
7. DiVincenzo, D. P. Quantum computation. *Science* **270**, 255–261 (1995).
8. Hegmann, F. A. *et al.* Time-resolved photoresponse of a gallium-doped germanium photoconductor using a variable-pulse-width terahertz source. *Appl. Phys. Lett.* **76**, 282–284 (2000).
9. Rabi, I. I. Space quantization in a gyrating magnetic field. *Phys. Rev.* **51**, 652–654 (1937).
10. Boyd, R. W. *Nonlinear Optics* (Academic, Boston, 1992).
11. Kohn, W. in *Solid State Physics* (eds Seitz, F. & Turnbull, D.) Vol. 5, 257–320 (Academic, New York, 1957).
12. Yu, P. Y. & Cardona, M. *Fundamentals of Semiconductors: Physics and Materials Properties* (Springer, Berlin, 1999).
13. Klemens, T. O., Dunn, I. L. & Bates, C. A. in *Atoms and Molecules in Strong External Fields* (eds Schuricht, P. & Schweizer, W.) 291–300 (Plenum, New York, 1998).
14. Stillman, G. E., Wolfe, C. M. & Dimmock, J. O. Magnetospectroscopy of shallow donors in GaAs. *Solid State Commun.* **7**, 921–925 (1969).
15. Burghoorn, J., Klaassen, T. O. & Wenckebach, W. T. The dynamics of shallow donor ionization in n-GaAs studied with sub-mm FIR-induced photoconductivity. *Semicond. Sci. Technol.* **9**, 30–34 (1994).
16. Larsen, D. M. Inhomogeneous line broadening in donor magneto-optical spectra. *Phys. Rev. B* **8**, 535–553 (1973).
17. Hunsche, S. *et al.* Far-infrared picosecond time-resolved measurement of the free-induction decay in GaAs:Si. *Phys. Rev. B* **51**, 9643–9647 (1995).
18. Cundiff, S. T. *et al.* Rabi flopping in semiconductors. *Phys. Rev. Lett.* **73**, 1178–1181 (1994).
19. Schaligin, A. *et al.* Direct observation of excitonic Rabi oscillations in semiconductors. *Phys. Rev. Lett.* **82**, 2346–2349 (1999).
20. Ramian, G. The new UCSB free-electron lasers. *Nucl. Instrum. Methods Phys. Res. A* **318**, 225–229 (1992).
21. Hegmann, F. A. & Sherwin, M. S. Generation of picosecond far-infrared pulses using laser activated semiconductor reflection switches. *Proc. SPIE* **2842**, 90–105 (1996).
22. Beckelmann, U. Phonon scattering between zero-dimensional electronic states: Spatial versus Landau quantization. *Phys. Rev. B* **50**, 17271–17279 (1994).
23. Barrie, R. & Nishikawa, K. Phonon broadening of impurity spectral lines II. Application to silicon. *Can. J. Phys.* **41**, 1823–1835 (1963).
24. Nishikawa, K. & Barrie, R. Phonon broadening of impurity spectral lines I. General theory. *Can. J. Phys.* **41**, 1135–1173 (1963).
25. Stanley, C. R. *et al.* Electrical characterization of molecular beam epitaxial GaAs with peak electron mobilities up to approximately $\sim 4 \times 10^5$ cm^2/V·s. *Appl. Phys. Lett.* **58**, 478–480 (1991).
26. Stanley, C. R., Holland, M. C., Hutchins, R. H., Xenos, A. H. & Johnson, N. P. in *Institute of Physics Conference Series* Vol. 112 (ed. Singer, K. E.) 67–72 (IOP Publishing, London, 1990).
27. McKnight, S. W., Stewart, K. P., Drew, H. D. & Moorjani, K. Wavelength-independent anti-interference coating for the far-infrared. *Infrared Phys.* **27**, 327–333 (1987).

Acknowledgements

We thank D. K. Enyeart and C. Sean Roy for assistance with experiments, and C. J. Weinberger, D. D. Awschalom, and A. Imamoglu for critical readings of the manuscript. This work was supported by the ARO, the ONR/Medical Free-Electron Laser Program, the NSF, and Sun Microsystems.

Correspondence and requests for materials should be addressed to M.S.S. (e-mail: sherwin@physics.ucsb.edu).

Superconductivity at 39 K in magnesium diboride

Jun Nagamatsu*, Norimasa Nakagawa*, Takahiro Muranaka*, Yuji Zenitani* & Jun Akimitsu*†

** Department of Physics, Aoyama-Gakuin University, Chitosedai, Setagaya-ku, Tokyo 157-8572, Japan*

† CREST, Japan Science and Technology Corporation, Kawaguchi, Saitama 332-0012, Japan

In the light of the tremendous progress that has been made in raising the transition temperature of the copper oxide superconductors (for a review, see ref. 1), it is natural to wonder how high the transition temperature, T_c, can be pushed in other classes of materials. At present, the highest reported values of T_c for non-copper-oxide bulk superconductivity are 33 K in electron-doped $Cs_xRb_yC_{60}$ (ref. 2), and 30 K in $Ba_{1-x}K_xBiO_3$ (ref. 3). (Hole-doped C_{60} was recently found[3] to be superconducting with a T_c as high as 52 K, although the nature of the experiment meant that the superconductivity was confined to the surface of the C_{60} crystal, rather than probing the bulk.) Here we report the discovery of bulk superconductivity in magnesium diboride, MgB_2. Magnetization and resistivity measurements establish a transition temperature of 39 K, which we believe to be the highest yet determined for a non-copper-oxide bulk superconductor.

The samples were prepared from powdered magnesium (Mg; 99.9%) and powdered amorphous boron (B; 99%) in a dry box. The powders were mixed in an appropriate ratio (Mg:B = 1:2), ground and pressed into pellets. The pellets were heated at 973 K

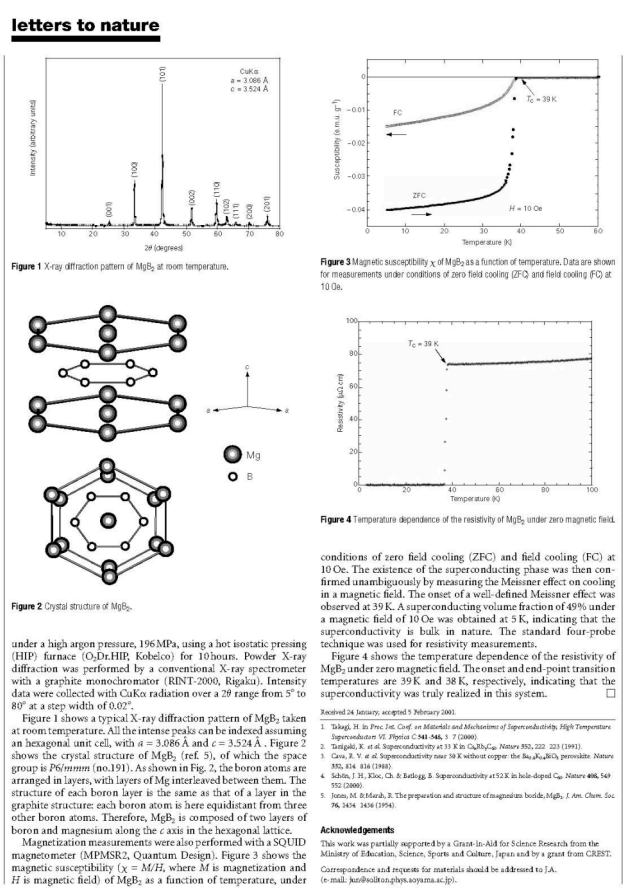

letters to nature

Figure 1 X-ray diffraction pattern of MgB_2 at room temperature.

Figure 2 Crystal structure of MgB_2.

under a high argon pressure, 196 MPa, using a hot isostatic pressing (HIP) furnace (O$_2$Dr.HIP, Kobelco) for 10 hours. Powder X-ray diffraction was performed by a conventional X-ray spectrometer with a graphite monochromator (RINT-2000, Rigaku). Intensity data were collected with CuKα radiation over a 2θ range from 5° to 80° at a step width of 0.02°.

Figure 1 shows a typical X-ray diffraction pattern of MgB_2 taken at room temperature. All the intense peaks can be indexed assuming an hexagonal unit cell, with $a = 3.086$ Å and $c = 3.524$ Å. Figure 2 shows the crystal structure of MgB_2 (ref. 5), of which the space group is *P6/mmm* (no.191). As shown in Fig. 2, the boron atoms are arranged in layers, with layers of Mg interleaved between them. The structure of each boron layer is the same as that of a layer in the graphite structure: each boron atom is here equidistant from three other boron atoms. Therefore, MgB_2 is composed of two layers of boron and magnesium along the c axis in the hexagonal lattice.

Magnetization measurements were also performed with a SQUID magnetometer (MPMSR2, Quantum Design). Figure 3 shows the magnetic susceptibility ($\chi = M/H$, where M is magnetization and H is magnetic field) of MgB_2 as a function of temperature, under

Figure 3 Magnetic susceptibility χ of MgB_2 as a function of temperature. Data are shown for measurements under conditions of zero field cooling (ZFC) and field cooling (FC) at 10 Oe.

Figure 4 Temperature dependence of the resistivity of MgB_2 under zero magnetic field.

conditions of zero field cooling (ZFC) and field cooling (FC) at 10 Oe. The existence of the superconducting phase was then confirmed unambiguously by measuring the Meissner effect on cooling in a magnetic field. The onset of a well-defined Meissner effect was observed at 39 K. A superconducting volume fraction of 49% under a magnetic field of 10 Oe was obtained at 5 K, indicating that the superconductivity is bulk in nature. The standard four-probe technique was used for resistivity measurements.

Figure 4 shows the temperature dependence of the resistivity of MgB_2 under zero magnetic field. The onset and end-point transition temperatures are 39 K and 38 K, respectively, indicating that the superconductivity was truly realized in this system. □

Received 24 January; accepted 5 February 2001.

1. Tokagi, H. in *Proc. Int. Conf. on Materials and Mechanisms of Superconductivity, High Temperature Superconductors VI. Physica C* **341–348**, 5–7 (2000).
2. Tarrigalo, K. *et al.* Superconductivity at 33 K in $Cs_xRb_yC_{60}$. *Nature* **352**, 222–223 (1991).
3. Cava, R. V. *et al.* Superconductivity near 30 K without copper: the $Ba_{0.6}K_{0.4}BiO_3$ perovskite. *Nature* **332**, 814–816 (1988).
4. Schön, J. H., Kloc, Ch. & Batlogg, B. Superconductivity at 52 K in hole-doped C_{60}. *Nature* **408**, 549–552 (2000).
5. Jones, M. & Marsh, R. The preparation and structure of magnesium boride, MgB_2. *J. Am. Chem. Soc.* **76**, 1434–1436 (1954).

Acknowledgements

This work was partially supported by a Grant-in-Aid for Science Research from the Ministry of Education, Science, Sports and Culture, Japan and by a grant from CREST.

Correspondence and requests for materials should be addressed to J.A. (e-mail: jun@solkot.phys.aoyama.ac.jp).

1911 Kammeringh Onnes
Hg 4.2K

MgB_2以前の金属間化合物
最高Tc=23K Nb_3Ge

1986 Bednorz ansdMuller
LaBaCuO　非BCS

BCSの壁　Tc<30K？

MB_2化合物の超伝導特性
は多く調べられていた

1970 Cooper
M=Y, Zr, Nb, Mo
NbB_2 3.87K, $Mo_{0.87}B_2$ ~11K

1979 Leyarovska
M=Ti, Zr, Hf, V, Nb, Ta,
Cr, Mo

応用上注目される理由

- 金属間化合物では最高のTc=39 K
  - Cryocoolerでの冷却
  - 液体水素冷却（1気圧下）20.39K
- 原料(B, Mg)が豊富で安価

Mineral	埋蔵量[G ton]	価格[$/kg]（1996）
Al	28.000	1.54
B	0.420	0.375
Mg	3.600	2.7～3.9
Nb	0.004	6.61
Sn	0.010	6～10
Ti	0.610	9.9

(Mineral Commodity Summaries (2005), (1997))

http://home.hiroshima-u.ac.jp/er/A_Japan_Sea/A3.PDF
http://home.hiroshima-u.ac.jp/er/A_Japan_Sea/T7.PDF
#search='金属%20価格'

線材としての問題点

- 物性面の理解は進んだ
- 現在の線材はNbベースの金属系超伝導体に比べて磁場中のJc特性が低い
- 「MgB2における臨界電流特性に関する調査研究会」 2005〜2007
- 結晶粒充填率が低い
- 結晶間結合が小さい（にもかかわらず超伝導線として働く）
- SiC添加でピン力向上をはかる

超伝導物質としてのMgB_2

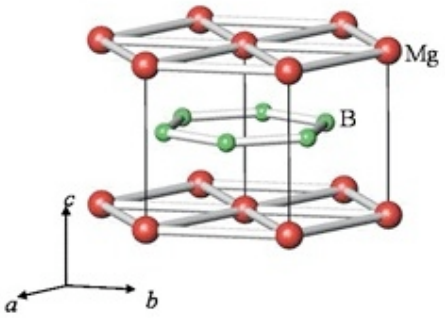

Fig.1 MgB_2の結晶構造

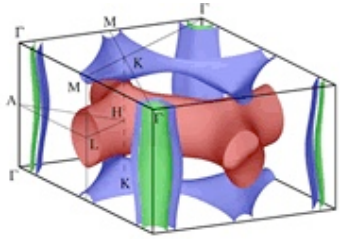

Fig.4 MgB_2のフェルミ面

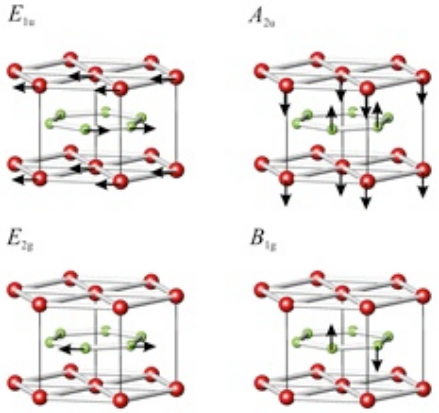

Fig.5 MgB_2のフォノンモード

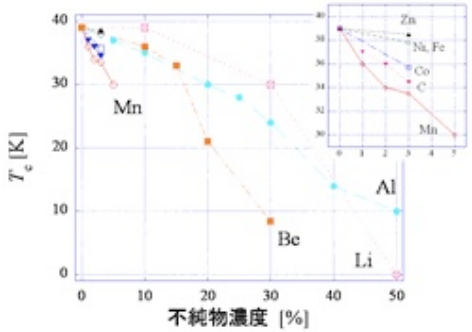

Fig.6 MgB_2の置換効果

（秋光研のHPから転載）

低充填率・低結晶結合の原因

MgB2生成反応での体積変化

$$Mg + 2B \rightarrow MgB_2$$

$$\frac{V_{Mg+2B}}{V_{MgB2}} = 0.74$$

左辺：13.97+2x4.914=23.80 cm^3/mol

右辺：17.53 cm^3/mol

	Mg	B	MgB2
密度[g/cm^3]	1.74	2.2	2.62
分子量[g/mol]	24.31	10.81	45.93
分子体積[cm^3/mol]	13.97	4.914	17.53

（理科年表　他）

MgB_2結晶表面と結晶間に存在するMgO

Mgの表面酸化物層

Bの表面のB_2O_3がMgで還元されて生じる

MgOは非常に安定な物資

充填率向上、MgO排除

Bのみに着目すればΔV=+7.70 cm^3/1mol MgB_2

Mg蒸気を拡散で反応させる（東大　下山研）

市販MgB_2から化学的にMgOを除去

安息香酸0.2Mベンゼン溶液＋熱処理（物材機構）

熱処理中にMgOを除去、
あるいはMgOの悪影響を無くすことはできないか？

酸化還元反応

$2Mg(solid) + O2(gas) \rightleftarrows 2MgO(solid)$

$4B(solid) + 3O2(gas) \rightleftarrows 2B2O3(solid)$

$$\Delta G^0 = RT\ Log[p_{O2}]$$

反応の自由エネルギー　温度　平衡酸素分圧

低酸素分圧雰囲気では反応は左向きに進む

固体電解質を用いた酸素ポンプ

高温（400℃<T）のZrO_2セラミックス中で酸素分子はイオン化する

$$O_2 \rightarrow 2O^{2-} - 4e^-$$

ZrO_2セラミックスの隔壁に電極を付けて外部から電圧を加えると
セラミックス中を通して酸素を輸送できる

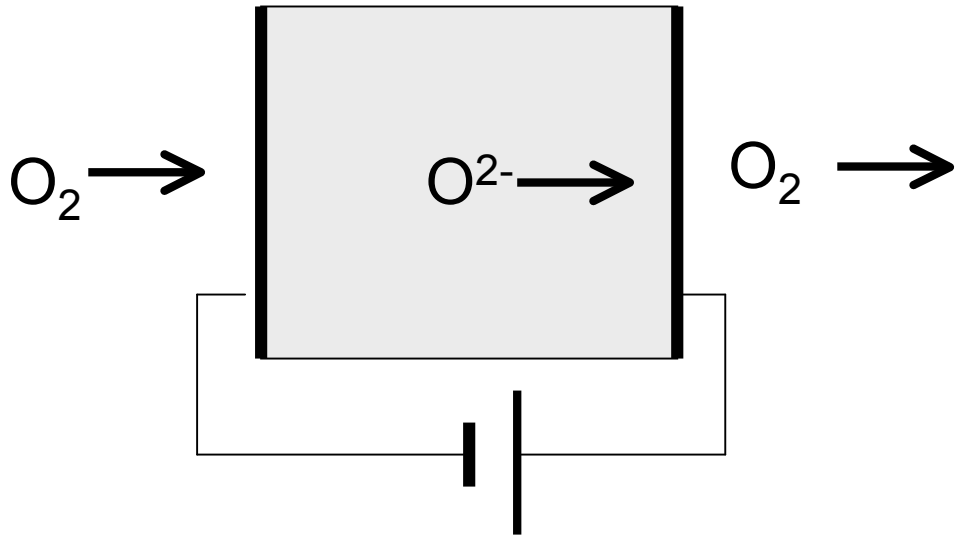

酸素ポンプ試作

od22mm, t3mmのイットリア安定化ジルコニア管
Ptペースト塗布/焼結　-> 多孔質電極
ϕ60アルミナ管を真空チェンバーとして、管状電気炉で加熱

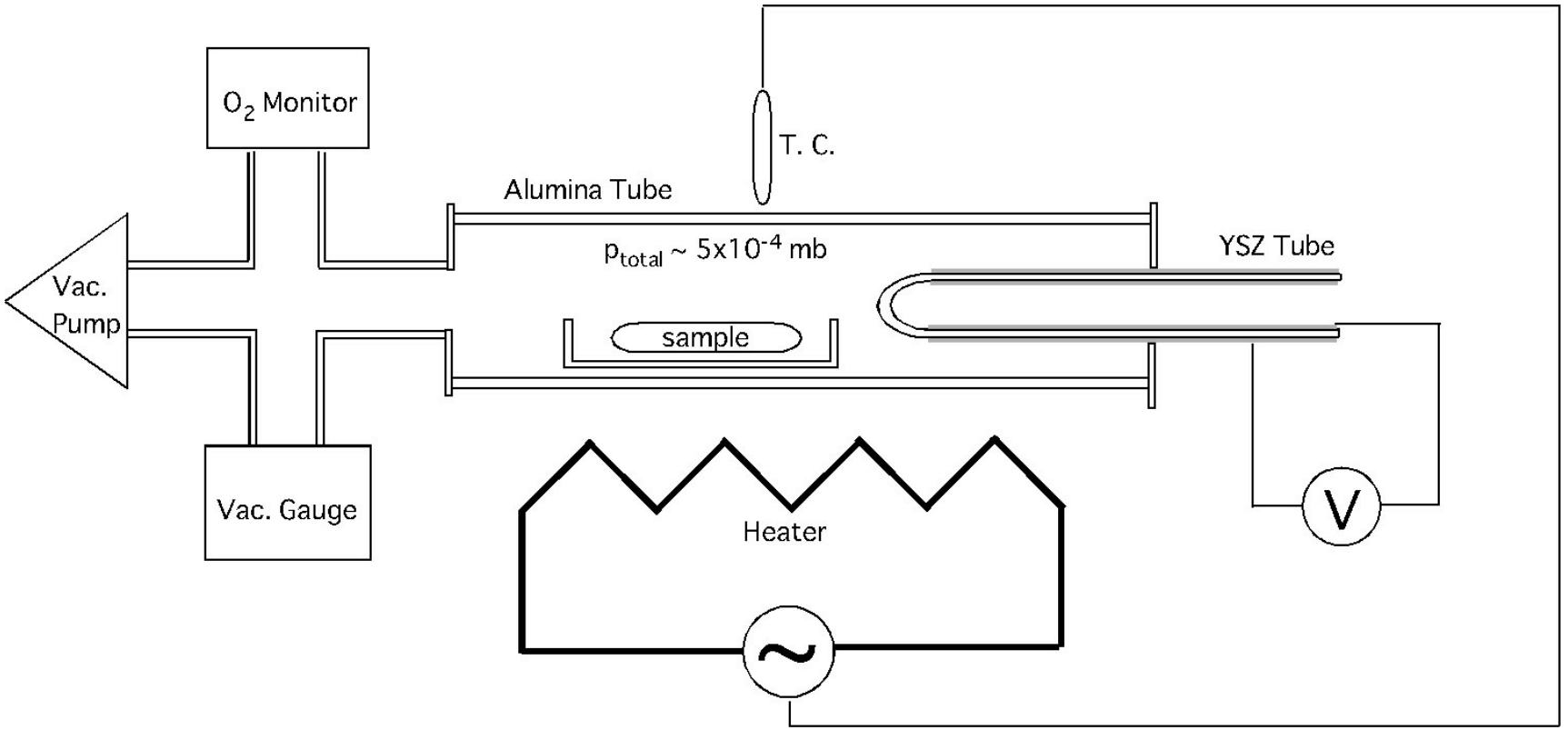

真空炉+酸素ポンプ

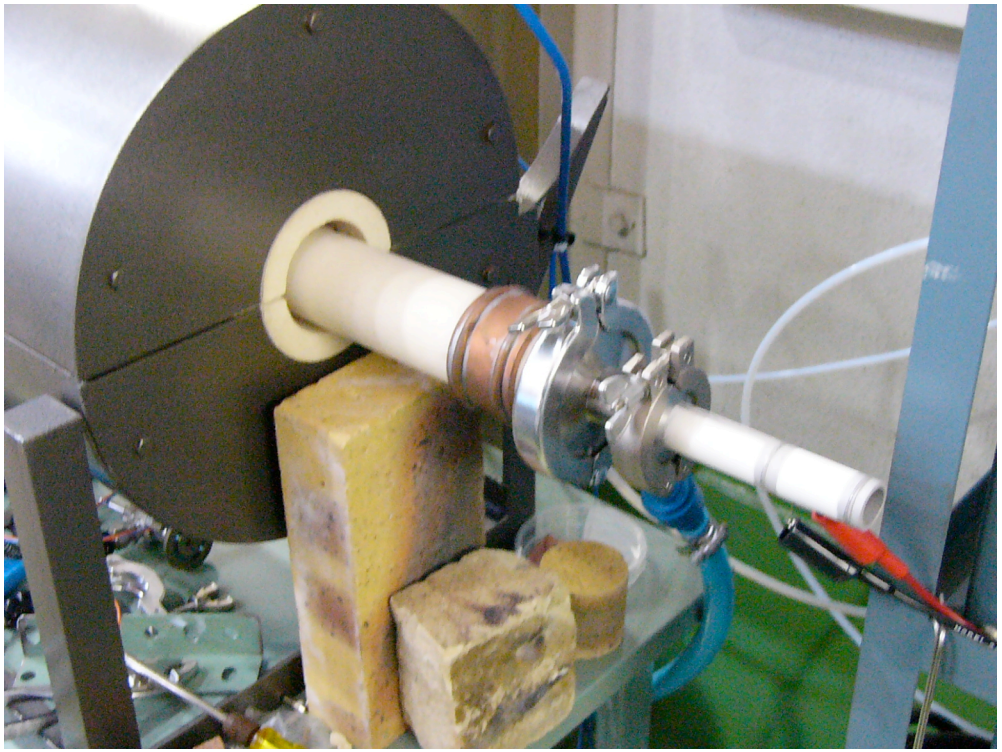

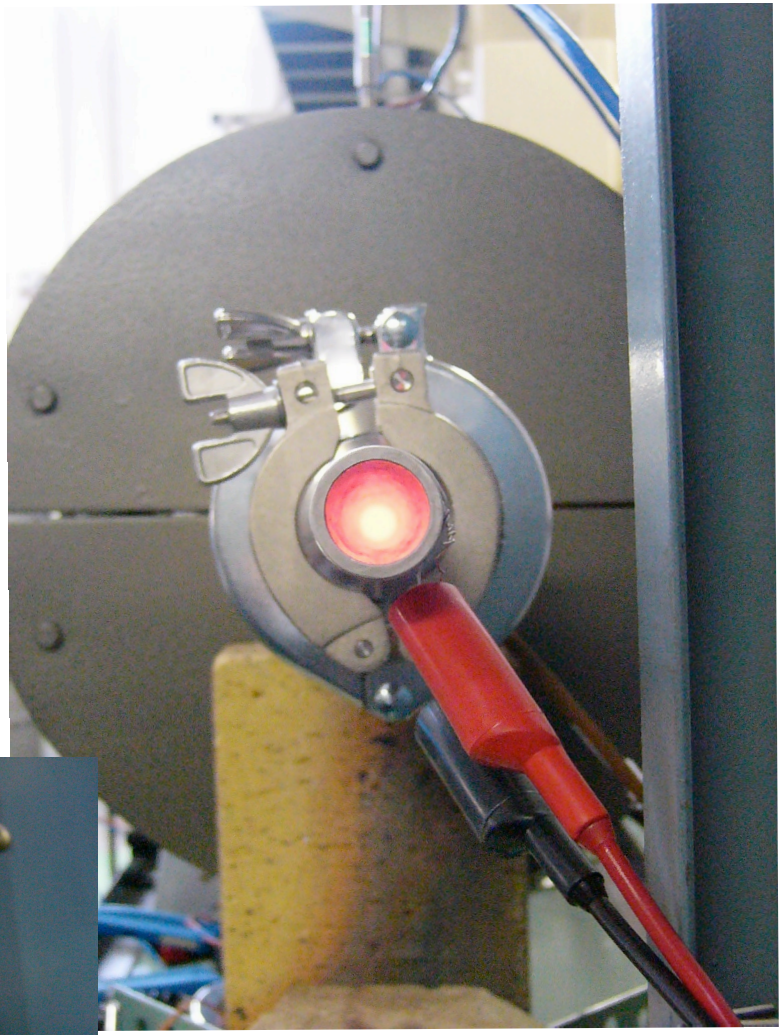

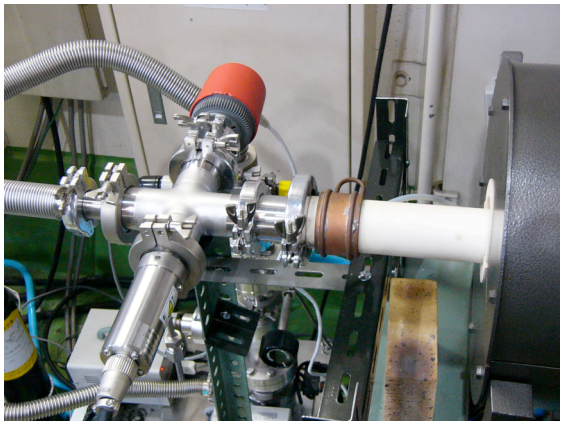

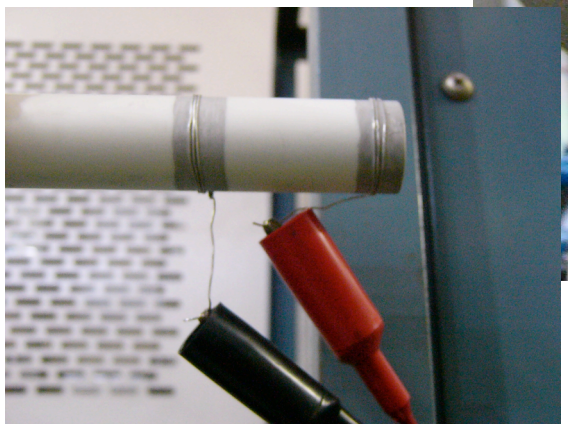

温度、真空度、酸素分圧

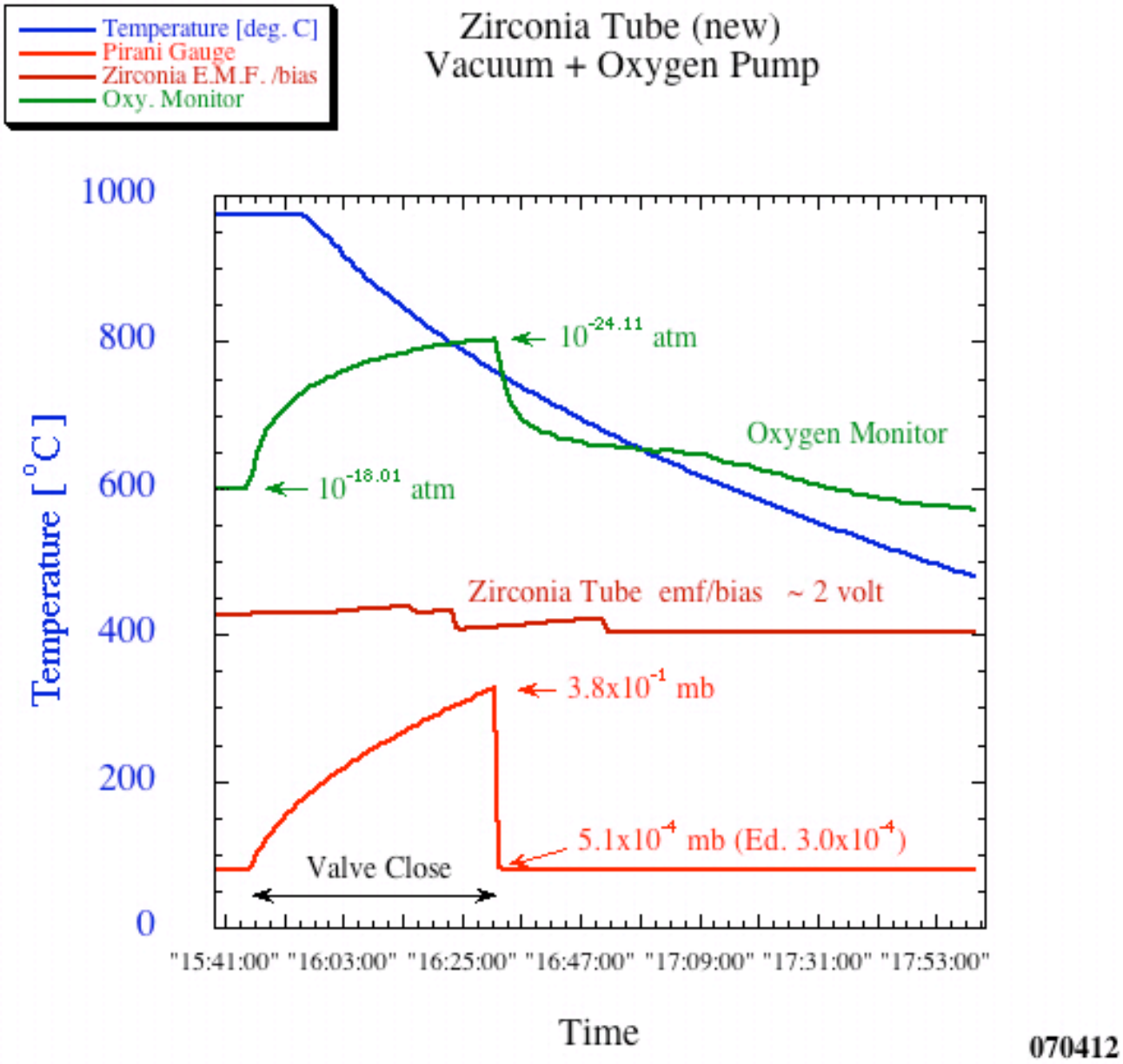
Temperature [deg. C]
Pirani Gauge
Zirconia E.M.F. /bias
Oxy. Monitor
Zirconia Tube (new)
Vacuum + Oxygen Pump
1000
800
600
400
200
0
Temperature [°C]
10^-24.11 atm
Oxygen Monitor
10^-18.01 atm
Zirconia Tube emf/bias ~ 2 volt
3.8x10^-1 mb
5.1x10^-4 mb (Ed. 3.0x10^-4)
Valve Close
"15:41:00" "16:03:00" "16:25:00" "16:47:00" "17:09:00" "17:31:00" "17:53:00"
Time
070412

金属酸化物還元例

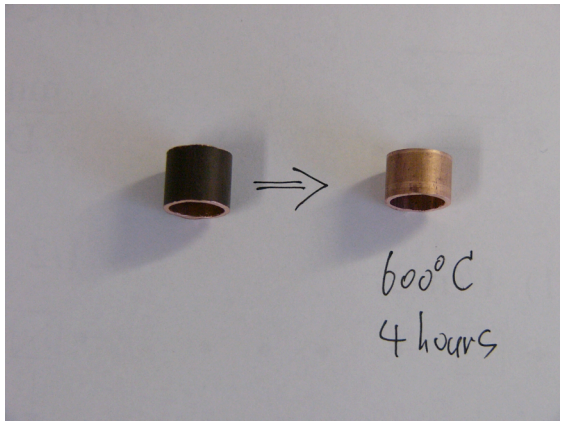

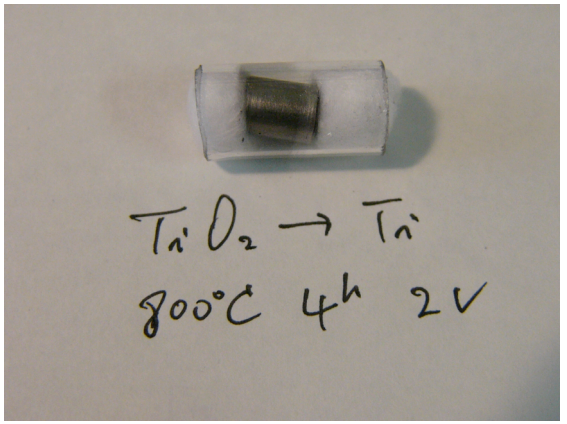

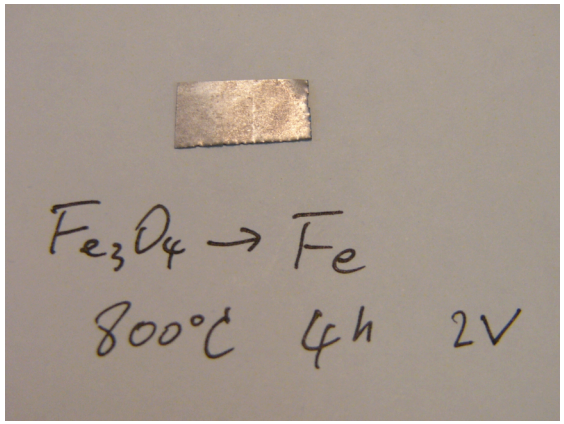

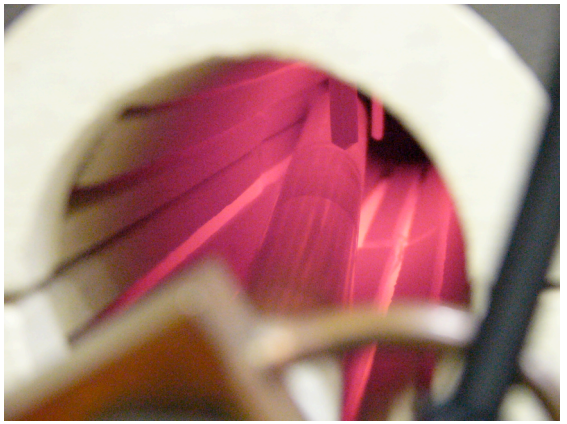

MgB2 bulk焼成例

PIT(Powder In Tube), in-situ, 1000℃　8時間

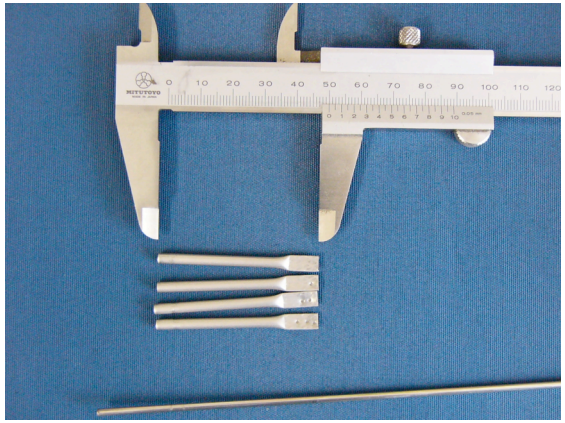

SUS ϕ3.4 t0.28

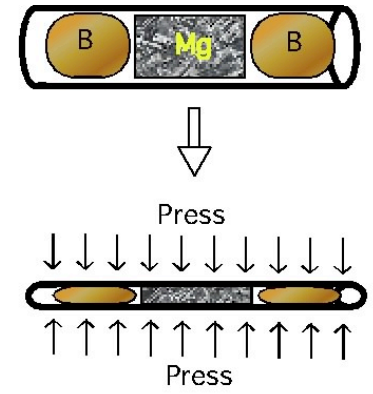

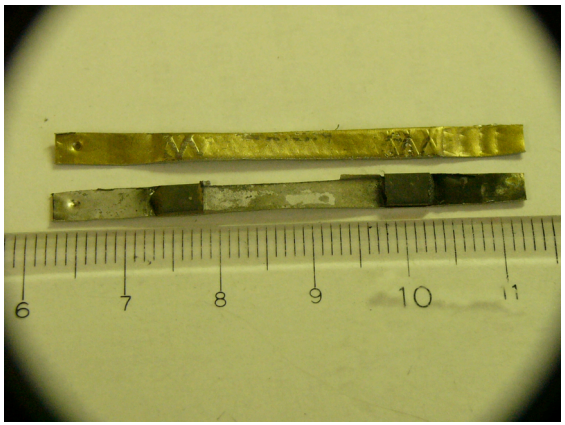

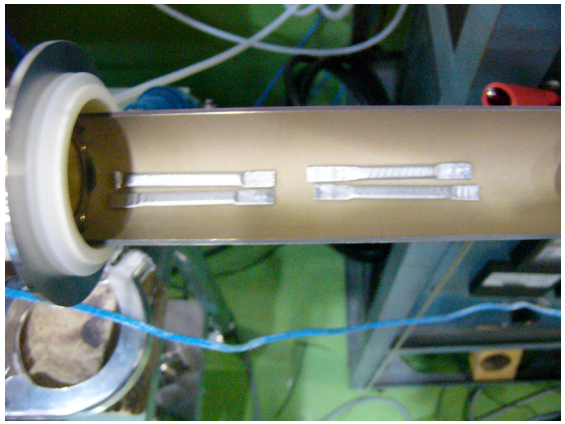

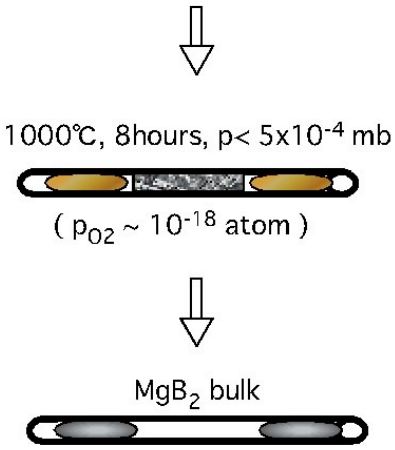

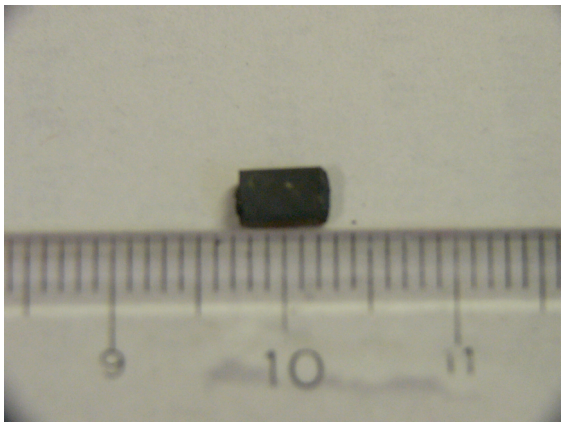

酸化物除去の可能性

$p_{O2} \approx 10^{-24}$ atom までは
酸素分圧を落とせる

酸素分圧一定
ΔG^0 - T 図上では傾き
R Log[p_{O2}] の直線

赤線より上方の範囲が
還元可能

MgOは難しいが
B_2O_3は可能性がある

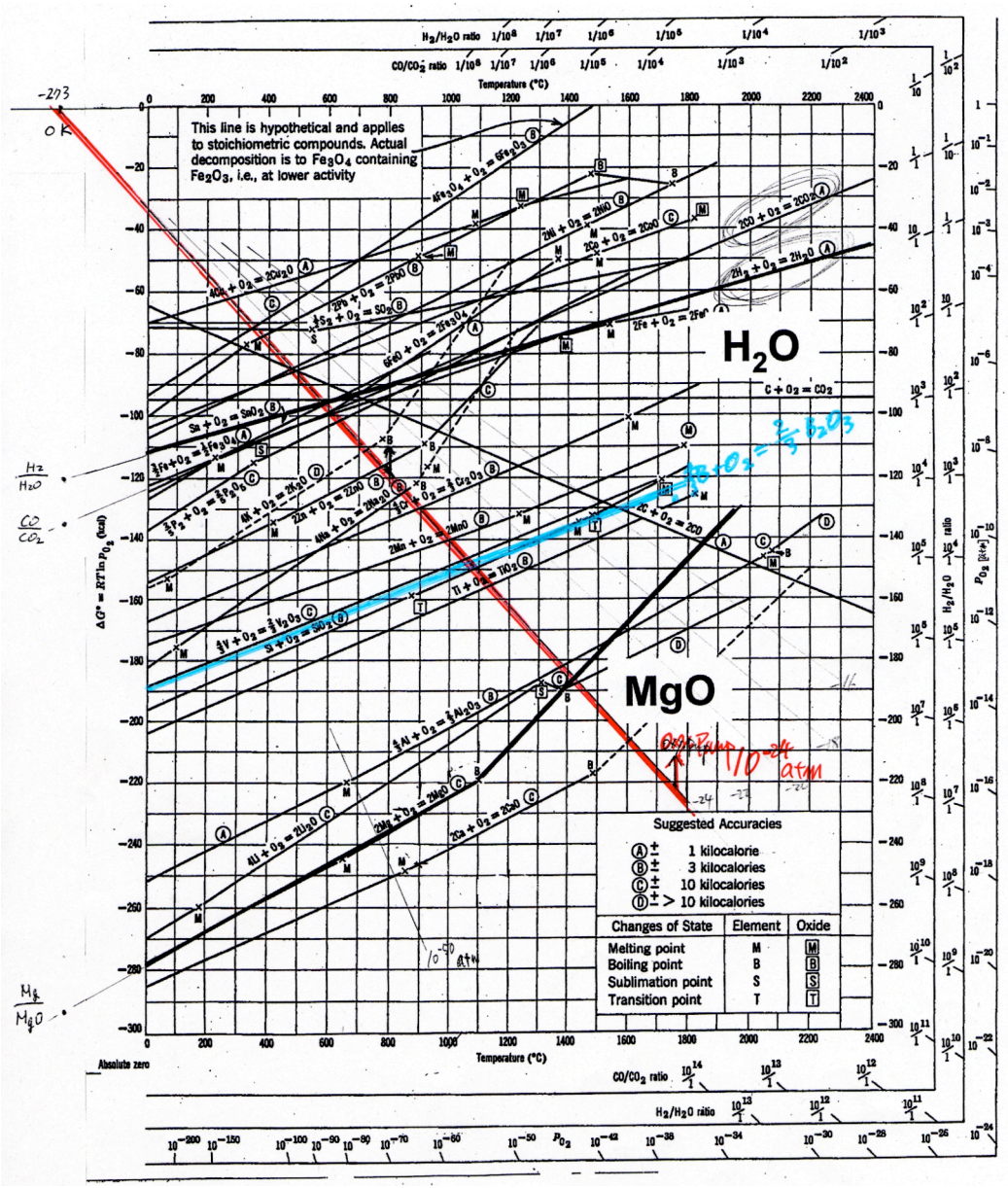

まとめと今後の課題

- 現在の酸素ポンプと電気炉の性能ではMgOの直接還元は難しい
- B表面の酸化物除去は可能性がある
- 表面に酸化物層を持たないBを原料にして、Mg蒸気の拡散で反応させ、MgOを含まないMgB_2生成をめざす
- 純MgB2からex-situ法で線材サンプルを作成し、Jc測定を行う